

Shear Stress Analysis in a Rotator-Stator System

Ricardo Serfaty¹, Bruno de Almeida Barbabela²,
Flávio Martins de Queiroz Guimarães² and Luiz Eduardo Ganem Rubião²

¹Petrobras/CENPES, Rio de Janeiro / RJ - Brazil
Phone: +55-21-3865-6209
e-mail: rserfaty@cenpes.petrobras.com.br

²Chemtech - A Siemens Company, Rio de Janeiro / RJ - Brazil
Phone: +55-21-2509-1114
e-mail: flavio.guimaraes@chemtech.com.br

Abstract

The present work describes the simulations performed to evaluate the surface tension on the test plates attached to a rotator-stator system (a rotating device submerged into a viscous medium). The system was considered symmetric along the vertical axis so just one eighth of the system has been simulated. Preliminary tuning of the model was achieved by comparing it with the exact algebraic solution for a cylindrical coordinate Couette like flow. For further use, the model parameters have been generalized and the system has been included into a human-machine interface for fast configuration of the simulations. Velocity gradients evaluation near the surface of the rotating plates was calculated with additional code implemented into GROUND file.

1. INTRODUCTION

The increasing safety, health and environmental awarenesses have motivated remarkable advances in industrial practices during the last years. The understanding of how equipments fail is a key point in the development of a Reliability Centered Maintenance (RMC) program, which, in the past few years, is been implemented in several companies in the oil and gas industry.

Computational fluid dynamics (CFD) has been applied successfully in many situations to supply a detailed insight view of equipments operation. Comparing to other types of mathematical models based mainly in statistical regressions or empirical correlations, CFD proved to be a much more realistic approach.

The extreme adverse media and high flow velocities during the operations in the petroleum exploitation and refining industry lead to a continuous problem concerning pipelines and rotating equipments. Investments in the study of special operating conditions receive therefore an important attention from companies in this industry as a way of minimizing impacts and assuring sustainable operation.

This work was dedicated to the development of a model for simulation of test plates attached to a rotating device submerged into a viscous medium. The focus of these simulations was to determine the shear stress on these surfaces.

2. DESCRIPTION OF THE SYSTEM AND MODELING

2.1. Geometry

The system consists of a vertical axis rotating device with eight test plates attached submerged into a viscous medium as shown in figure 1 below. Since the system can be considered axial symmetric, just one eighth of it has been simulated.

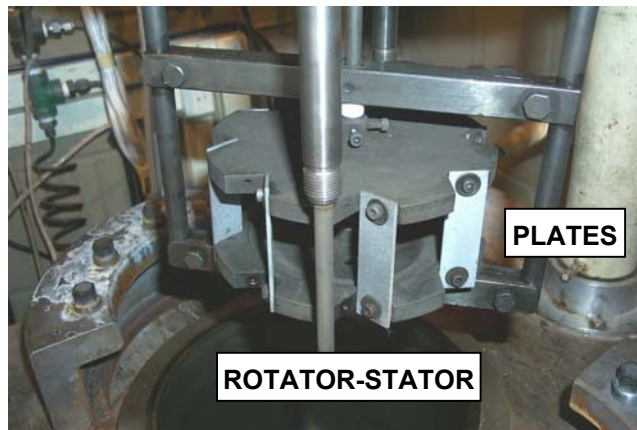


Figure 1 - System geometry

2.2. Properties

Density

The fluid consists, basically, of a mixture of hydrocarbons. Since the composition of the mixture was considered constant and the fluid is incompressible, no density change is expected so it was defined as constant along the domain.

Viscosity

In this first approach the laminar viscosity of the fluid was also defined as constant along the computational domain.

Roughness

The surface of the test plates were considered regular, plane and homogenous. Then, the roughness was considered constant along all faces.

2.3. Sources and Environmental conditions

Turbulence

The Low-Reynolds Wilcox $K-\omega$ model was used. The turbulent viscosity was calculated using the Kolmogorov's frequency model.

3. MATHEMATICAL MODELING

3.1. Computational grid

The domain definition was one of the major steps of the system setting-up. It was created as a two-blocks body-fitted grid with a sliding interface between the blocks. Figure 2 below shows the grid nodes for a general XY plane.

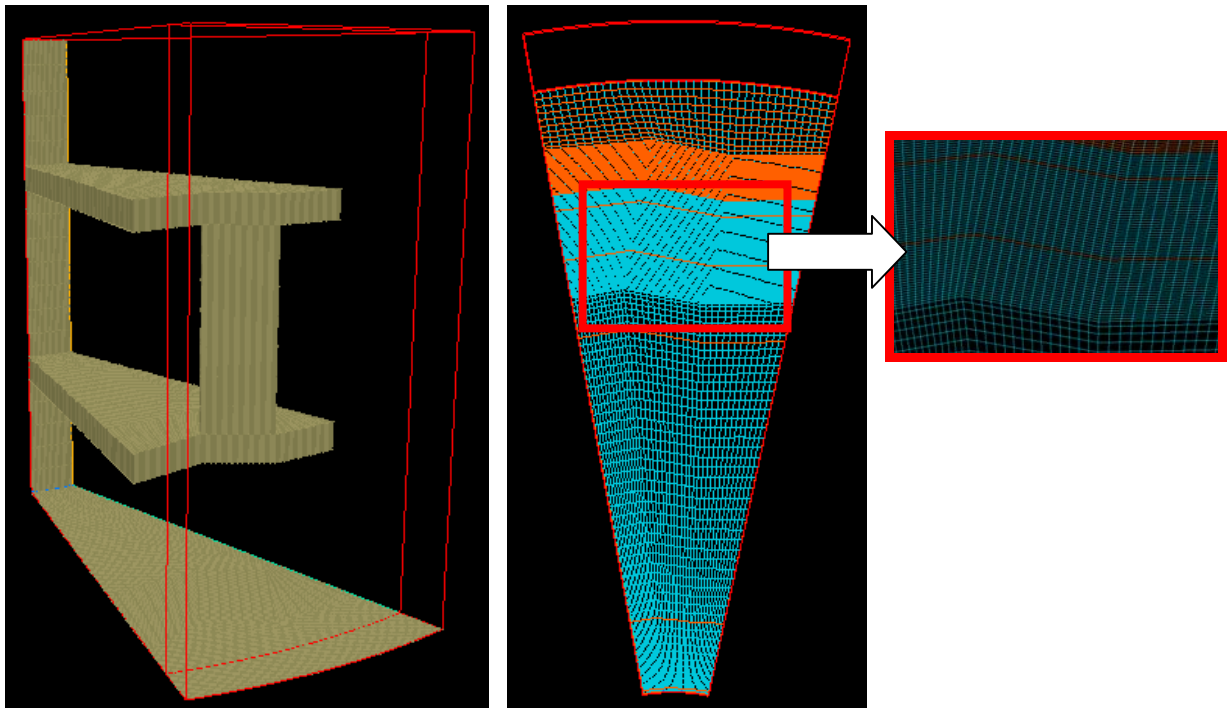


Figure 2 - Grid nodes at XY plane

3.2. Rotation

The multi-block sliding-grid option was used to include the rotating sources into the system.

3.3. Relaxation

Relaxation was implemented into GROUND based on in-cells residence times. Since the main flow occurs in one direction only (angular one), the angular velocity component needs more relaxation than the others. So, different formulas have been implemented based on each direction residence time.

3.4. Equation formulation

The General Collocated Velocity method (GCV) was selected to be as the solution procedure for the Navier-Stokes equations. For this particular system this algorithm has shown a faster and more stable convergence profile than the standard elliptic-staggered one.

3.5. Shear stress calculation

For the evaluation of the near wall velocity gradients, a finite-elements approach with a 6 (six) nodes quadrilateral element was used.

A bidimensional local coordinate system (R and S directions) was defined based on the heterogeneous derivatives. These calculation planes are shown in Table 1 below:

Table 1 - Local coordinates planes

x-direction	$\frac{\partial U}{\partial y} \Rightarrow R = f(y); S = f(x)$	$\frac{\partial U}{\partial z} \Rightarrow R = f(z); S = f(x)$
y-direction	$\frac{\partial V}{\partial x} \Rightarrow R = f(x); S = f(y)$	$\frac{\partial V}{\partial z} \Rightarrow R = f(z); S = f(y)$
z-direction	$\frac{\partial W}{\partial x} \Rightarrow R = f(x); S = f(z)$	$\frac{\partial W}{\partial y} \Rightarrow R = f(y); S = f(z)$

Partial derivative calculation

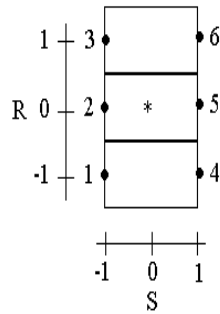
Inside the region of the current element, the value of a variable is a sum of the values of the same variable at the node points pondered by the shape functions. These shape functions are designed to be equal to unity at their actual node points and to zero at the other ones. For the solution of the gradient profile, the partial derivatives are solved as a sum of the variable node values pondered by the shape functions derived in respect to the spatial coordinates.

$$\phi = \sum_k N_k \phi_k$$

$$\frac{\partial \phi}{\partial y} = \sum_k \frac{\partial N_k}{\partial y} \phi_k \quad \rightarrow \quad \frac{\partial N_k}{\partial y} = \frac{\partial N_k}{\partial R} \frac{\partial R}{\partial y} = \frac{\partial N_k}{\partial R} \left(\frac{1}{\Delta y} \right)$$

For the calculation of the shape functions three kinds of finite-elements were defined: one for the elements without wall contact; one for the elements where the lower face is blocked; and the other for the elements where the upper face is blocked. For the last two cases it was assumed that exists a fine layer very close to the wall which have the same momentum profile of the moving object.

First Case: No wall contact



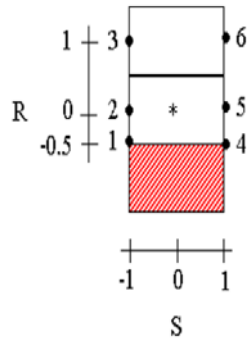
$$R = \left(\frac{y - y_0}{\Delta y} \right)$$

$$S = 2 \left(\frac{x - x_0}{\Delta x} \right)$$

Shape Functions

$N_1 = -\frac{R(1-R)(1-S)}{4}$	$\frac{\partial N_1}{\partial R} = \frac{(2R-1)(1-S)}{4}$		$\frac{\partial N_1}{\partial R} = -\frac{1}{4}$
$N_2 = \frac{(1+R)(1-R)(1-S)}{2}$	$\frac{\partial N_2}{\partial R} = -\frac{2R(1-S)}{2}$	$R = 0$	$\frac{\partial N_2}{\partial R} = 0$
$N_3 = \frac{R(1+R)(1-S)}{4}$	$\frac{\partial N_3}{\partial R} = \frac{(2R+1)(1-S)}{4}$	\Rightarrow	$\frac{\partial N_3}{\partial R} = \frac{1}{4}$
$N_4 = -\frac{R(1-R)(1+S)}{4}$	$\frac{\partial N_4}{\partial R} = \frac{(2R-1)(1+S)}{4}$	$S = 0$	$\frac{\partial N_4}{\partial R} = -\frac{1}{4}$
$N_5 = \frac{(1+R)(1-R)(1+S)}{2}$	$\frac{\partial N_5}{\partial R} = -\frac{2R(1+S)}{2}$		$\frac{\partial N_5}{\partial R} = 0$
$N_6 = \frac{R(1+R)(1+S)}{4}$	$\frac{\partial N_6}{\partial R} = \frac{(2R+1)(1+S)}{4}$		$\frac{\partial N_6}{\partial R} = \frac{1}{4}$

Second Case: Lower wall

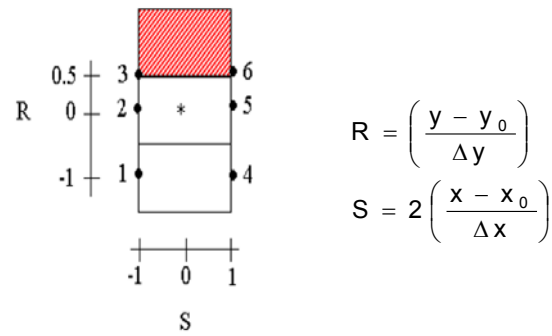


$$R = \left(\frac{y - y_0}{\Delta y} \right)$$

$$S = 2 \left(\frac{x - x_0}{\Delta x} \right)$$

Shape Functions

$N_1 = -\frac{2R(1-R)(1-S)}{3}$	$\frac{\partial N_1}{\partial R} = \frac{2(2R-1)(1-S)}{3}$		$\frac{\partial N_1}{\partial R} = -\frac{2}{3}$
$N_2 = (0.5+R)(1-R)(1-S)$	$\frac{\partial N_2}{\partial R} = (0.5-2R)(1-S)$	$R = 0$	$\frac{\partial N_2}{\partial R} = \frac{1}{2}$
$N_3 = \frac{R(0.5+R)(1-S)}{3}$	$\frac{\partial N_3}{\partial R} = \frac{(0.5+2R)(1-S)}{3}$	\Rightarrow	$\frac{\partial N_3}{\partial R} = \frac{1}{6}$
$N_4 = -\frac{2R(1-R)(1+S)}{3}$	$\frac{\partial N_4}{\partial R} = \frac{2(2R-1)(1+S)}{3}$	$S = 0$	$\frac{\partial N_4}{\partial R} = -\frac{2}{3}$
$N_5 = (0.5+R)(1-R)(1+S)$	$\frac{\partial N_5}{\partial R} = (0.5-2R)(1+S)$		$\frac{\partial N_5}{\partial R} = \frac{1}{2}$
$N_6 = \frac{R(0.5+R)(1+S)}{3}$	$\frac{\partial N_6}{\partial R} = \frac{(0.5+2R)(1+S)}{3}$		$\frac{\partial N_6}{\partial R} = \frac{1}{6}$

Third Case: Upper wallShape Functions

$$\begin{aligned}
 N_1 &= -\frac{R(0.5-R)(1-S)}{3} & \frac{\partial N_1}{\partial R} &= \frac{(2R-0.5)(1-S)}{3} & \frac{\partial N_1}{\partial R} &= -\frac{1}{6} \\
 N_2 &= (1+R)(0.5-R)(1-S) & \frac{\partial N_2}{\partial R} &= -(0.5+2R)(1-S) & R=0 & \frac{\partial N_2}{\partial R} &= -\frac{1}{2} \\
 N_3 &= \frac{2R(1+R)(1-S)}{3} & \frac{\partial N_3}{\partial R} &= \frac{2(2R+1)(1-S)}{3} & \implies & \frac{\partial N_3}{\partial R} &= \frac{2}{3} \\
 N_4 &= -\frac{R(0.5-R)(1+S)}{3} & \frac{\partial N_4}{\partial R} &= \frac{(2R-0.5)(1+S)}{3} & S=0 & \frac{\partial N_4}{\partial R} &= -\frac{1}{6} \\
 N_5 &= (1+R)(0.5-R)(1+S) & \frac{\partial N_5}{\partial R} &= -(0.5+2R)(1+S) & & \frac{\partial N_5}{\partial R} &= -\frac{1}{2} \\
 N_6 &= \frac{2R(1+R)(1+S)}{3} & \frac{\partial N_6}{\partial R} &= \frac{2(2R+1)(1+S)}{3} & & \frac{\partial N_6}{\partial R} &= \frac{2}{3}
 \end{aligned}$$

Shear stress calculation

With the spatial derivatives and the fluid viscosity it is possible to calculate the near wall shear stress using the following formulas:

$$\tau_{xy} = \tau_{yx} = -\mu \left[\frac{\partial v_x}{\partial y} + \frac{\partial v_y}{\partial x} \right]$$

$$\tau_{xz} = \tau_{zx} = -\mu \left[\frac{\partial v_x}{\partial z} + \frac{\partial v_z}{\partial x} \right]$$

$$\tau_{yz} = \tau_{zy} = -\mu \left[\frac{\partial v_y}{\partial z} + \frac{\partial v_z}{\partial y} \right]$$

4. VALIDATION

4.1. Methodology

For validation of the mathematical models, a Couette like flow has been evaluated. This simulation consisted of the flow in the gap region between two concentric cylinders with the inner cylinder rotating with constant angular velocity, as shown in Figure 3 below:

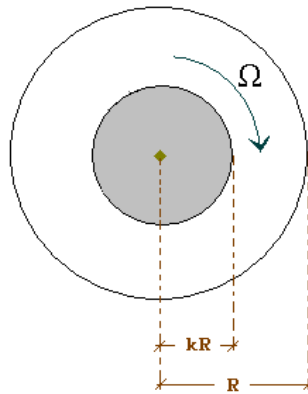


Figure 3 - Couette flow (cylindrical coordinates)

For an ideal flow, the two assumptions below are taken as true:

- In steady-state laminar flow, fluid moves following a fully circular profile with null radial and axial velocity components.
- Since the system is axially symmetric, the pressure gradient in the angular direction is considered null.

The Navier-Stokes equations in cylindrical-polar coordinates with constant density and viscosity are as follow:

- Angular component (θ):

$$\rho \left(\frac{\partial v_\theta}{\partial t} + v_r \frac{\partial v_\theta}{\partial r} + \frac{v_\theta}{r} \frac{\partial v_\theta}{\partial r} - \frac{v_r v_\theta}{r} + v_z \frac{\partial v_\theta}{\partial z} \right) = -\frac{1}{r} \frac{\partial p}{\partial \theta} + \mu \left[\frac{\partial}{\partial r} \left(\frac{1}{r} \frac{\partial}{\partial r} (r v_\theta) \right) + \frac{1}{r^2} \frac{\partial^2 v_\theta}{\partial \theta^2} + \frac{2}{r^2} \frac{\partial v_r}{\partial \theta} + \frac{\partial^2 v_\theta}{\partial z^2} \right] + \rho g_\theta$$

- Radial component (r):

$$\rho \left(\frac{\partial v_r}{\partial t} + v_r \frac{\partial v_r}{\partial r} + \frac{v_\theta}{r} \frac{\partial v_r}{\partial r} - \frac{v_\theta^2}{r} + v_z \frac{\partial v_r}{\partial z} \right) = -\frac{\partial p}{\partial r} + \mu \left[\frac{\partial}{\partial r} \left(\frac{1}{r} \frac{\partial}{\partial r} (r v_r) \right) + \frac{1}{r^2} \frac{\partial^2 v_r}{\partial \theta^2} - \frac{2}{r^2} \frac{\partial v_\theta}{\partial \theta} + \frac{\partial^2 v_r}{\partial z^2} \right] + \rho g_r$$

- Axial component (z):

$$\rho \left(\frac{\partial v_z}{\partial t} + v_r \frac{\partial v_z}{\partial r} + \frac{v_\theta}{r} \frac{\partial v_z}{\partial r} + v_z \frac{\partial v_z}{\partial z} \right) = -\frac{\partial p}{\partial z} + \mu \left[\frac{1}{r} \frac{\partial}{\partial r} \left(r \frac{\partial v_z}{\partial r} \right) + \frac{1}{r^2} \frac{\partial^2 v_z}{\partial \theta^2} + \frac{\partial^2 v_z}{\partial z^2} \right] + \rho g_z$$

For a Couette flow in the gap region:

θ component	r component	z component
$0 = \frac{\partial}{\partial r} \left(\frac{1}{r} \frac{\partial}{\partial r} (rv_\theta) \right)$	$-\rho \frac{v_\theta^2}{r} = -\frac{\partial p}{\partial r}$	$0 = -\frac{\partial p}{\partial z} + \rho g_z$

With the below boundary conditions for the case of the inner cylinder rotating with angular velocity Ω and the outer cylinder stationary:

- For $r = kR$ (internal rotating cylinder), $v_\theta = \Omega kR$;
- For $r = R$ (external cylinder), $v_\theta = 0$.

Integrating the angular component between the boundary conditions limits above:

$$\frac{d}{dr} \left(\frac{1}{r} \frac{d}{dr} (rv_\theta) \right) = 0 \Rightarrow v_\theta = \frac{\Omega kr}{(k^2 - 1)} - \frac{\Omega kR^2}{(k^2 - 1)r}$$

$$v_\theta = \Omega kR \frac{\left(\frac{r}{R} - \frac{R}{r} \right)}{k \left(k - \frac{1}{k} \right)}$$

The shear stress components in cylindrical coordinates are:

$$\tau_{r\theta} = \tau_{\theta r} = -\mu \left[r \frac{\partial}{\partial r} \left(\frac{v_\theta}{r} \right) + \frac{1}{r} \frac{\partial v_r}{\partial \theta} \right]$$

$$\tau_{\theta z} = \tau_{z\theta} = -\mu \left[\frac{\partial v_\theta}{\partial z} + \frac{1}{r} \frac{\partial v_z}{\partial \theta} \right]$$

$$\tau_{zr} = \tau_{rz} = -\mu \left[\frac{\partial v_z}{\partial r} + \frac{\partial v_r}{\partial z} \right]$$

For a Couette flow in the gap region: $\tau_{\theta z} = \tau_{z\theta} = 0$ e $\tau_{zr} = \tau_{rz} = 0$

$$\tau_{r\theta} = 2\rho\nu_L\Omega R^2 \left(\frac{1}{r^2} \right) \left(\frac{k}{1-k^2} \right)$$

4.2. Validation results

A simulation was built based on the same assumptions described on sections 2 and 3 above. This simulation was performed for an specific set of physical-chemical properties at a constant rotating speed of 100 RPM. Since the analytical solution is laminar, no turbulence model was considered in the simulation. The resulting profile is shown on Figure 4 below:

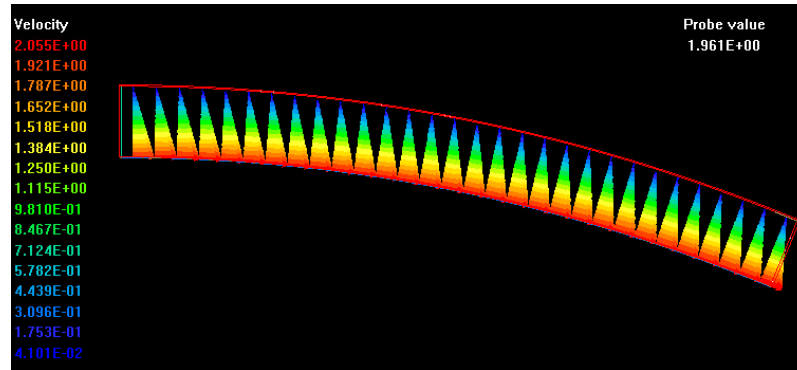


Figure 4 - Couette flow velocity profile (100 RPM)

Further, the analytical equations described in section 4.1 were solved with the same settings of the above PHOENICS simulation. The velocity profile and the rotating wall shear stress were compared for both cases in order to verify the precision of the system.

Table 2 - Couette flow shear stress results.

Case	Shear Stress (Pa)	Deviation (%)
Analytical	0.047	-
Simulation (dU/dY derivative)	0.042	-10.6
Simulation (all derivatives)	0.058	23.4

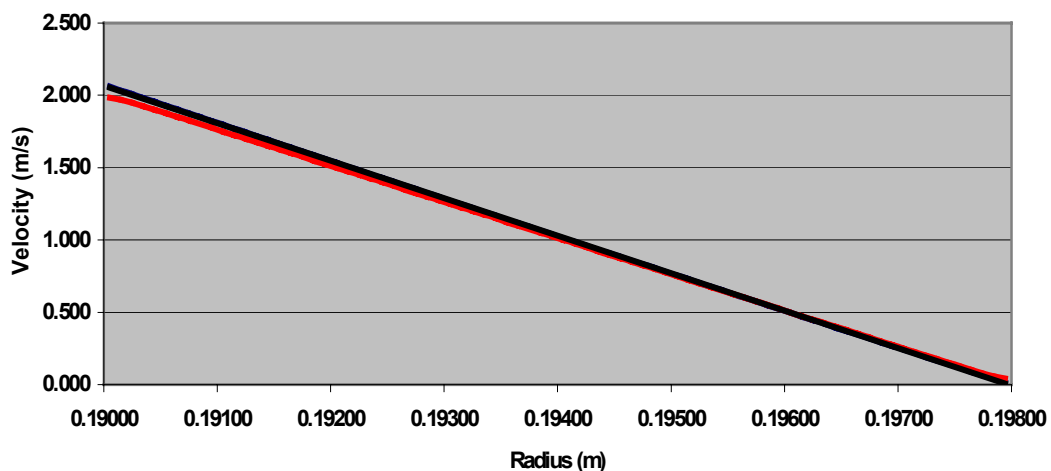


Figure 5 - Couette flow velocity profile: simulation (red) and analytical (black).

5. RESULTS AND DISCUSSION

To provide more detailed and easy to get information about the resulting shear stress profile, additional code was programmed into GROUND file to print treated data to the end of the RESULT file. The following information is provided:

- Average shear stress on the south surface of the plate (SAVG_in);
- Average shear stress on the north surface of the plate (SAVG_out);
- Shear stress at the center of the plate on the south surface (SHST_in);
- Shear stress at the center of the plate on the north surface (SHST_out);
- Shear stress at each cell of the south surface (slab by slab);
- Shear stress at each cell of the north surface (slab by slab);

The following lines gives some example of the results for a typical simulation:

```
BEGIN OF INTERFACE DATA
*****
Average Shear Stress:
SAVG_in = 1.793485E+01
SAVG_out= 1.857227E+01
Shear Stress at the Center:
SHST_in = 1.459734E+01
SHST_out= 1.423036E+01
*****
SHEAR STRESS AT INNER FACE:
IZ      =      7
2.645623E+01  1.799516E+01  1.621437E+01  1.538716E+01  1.492830E+01  1.466052E+01
1.452343E+01  1.450787E+01  1.462002E+01  1.488292E+01  1.539952E+01  1.650586E+01
1.973062E+01  3.584027E+01
IZ      =      8
2.613050E+01  1.793332E+01  1.618652E+01  1.537371E+01  1.492195E+01  1.465866E+01
1.452493E+01  1.451216E+01  1.462599E+01  1.489021E+01  1.540617E+01  1.650332E+01
1.966823E+01  3.493469E+01
IZ      =      9
2.620439E+01  1.796202E+01  1.620551E+01  1.538870E+01  1.493498E+01  1.467083E+01
1.453707E+01  1.452491E+01  1.464007E+01  1.490658E+01  1.542627E+01  1.653015E+01
1.972016E+01  3.507176E+01
IZ      =     10
2.629415E+01  1.799183E+01  1.622474E+01  1.540405E+01  1.494781E+01  1.468190E+01
1.454708E+01  1.453438E+01  1.464962E+01  1.491675E+01  1.543812E+01  1.654577E+01
1.975419E+01  3.519273E+01
IZ      =     11
2.634596E+01  1.801174E+01  1.623825E+01  1.541466E+01  1.495650E+01  1.468928E+01
1.455349E+01  1.454014E+01  1.465503E+01  1.492215E+01  1.544394E+01  1.655307E+01
1.977092E+01  3.525600E+01
IZ      =     12
2.637338E+01  1.802259E+01  1.624578E+01  1.542058E+01  1.496124E+01  1.469312E+01
1.455659E+01  1.454264E+01  1.465704E+01  1.492380E+01  1.544538E+01  1.655469E+01
1.977600E+01  3.528027E+01
IZ      =     13
2.637872E+01  1.802613E+01  1.624847E+01  1.542255E+01  1.496257E+01  1.469385E+01
1.455676E+01  1.454225E+01  1.465610E+01  1.492226E+01  1.544320E+01  1.655177E+01
1.977205E+01  3.527359E+01
IZ      =     14
2.636334E+01  1.802307E+01  1.624666E+01  1.542080E+01  1.496060E+01  1.469153E+01
1.455399E+01  1.453893E+01  1.465207E+01  1.491734E+01  1.543709E+01  1.654386E+01
1.975830E+01  3.523384E+01
IZ      =     15
2.632414E+01  1.801184E+01  1.623962E+01  1.541467E+01  1.495487E+01  1.468569E+01
1.454783E+01  1.453221E+01  1.464444E+01  1.490836E+01  1.542612E+01  1.652948E+01
```

```

1.973149E+01 3.515106E+01
IZ = 16
2.625193E+01 1.798916E+01 1.622510E+01 1.540279E+01 1.494429E+01 1.467584E+01
1.453809E+01 1.452199E+01 1.463317E+01 1.489537E+01 1.541021E+01 1.650815E+01
1.968899E+01 3.501210E+01
IZ = 17
2.615796E+01 1.795308E+01 1.620129E+01 1.538420E+01 1.492892E+01 1.466258E+01
1.452598E+01 1.451035E+01 1.462120E+01 1.488216E+01 1.539442E+01 1.648694E+01
1.964455E+01 3.488905E+01
IZ = 18
2.645447E+01 1.799486E+01 1.621423E+01 1.538703E+01 1.492819E+01 1.466046E+01
1.452337E+01 1.450783E+01 1.461989E+01 1.488287E+01 1.539949E+01 1.650583E+01
1.973046E+01 3.583945E+01
*****
SHEAR STRESS AT OUTTER FACE:
IZ = 7
2.862020E+01 1.729599E+01 1.502061E+01 1.399251E+01 1.351841E+01 1.336024E+01
1.338339E+01 1.351251E+01 1.376440E+01 1.425211E+01 1.516474E+01 1.697489E+01
2.157301E+01 4.529932E+01
IZ = 8
2.973689E+01 1.837613E+01 1.594415E+01 1.478873E+01 1.418455E+01 1.389339E+01
1.380855E+01 1.388174E+01 1.412002E+01 1.458563E+01 1.542661E+01 1.706710E+01
2.123700E+01 4.163072E+01
IZ = 9
3.020453E+01 1.874562E+01 1.627920E+01 1.509700E+01 1.445863E+01 1.412819E+01
1.400457E+01 1.404541E+01 1.425620E+01 1.469025E+01 1.548901E+01 1.707193E+01
2.118550E+01 4.129275E+01
IZ = 10
3.041603E+01 1.888975E+01 1.640844E+01 1.521804E+01 1.456781E+01 1.422271E+01
1.408381E+01 1.411051E+01 1.430874E+01 1.472947E+01 1.551358E+01 1.708125E+01
2.119705E+01 4.130908E+01
IZ = 11
3.051626E+01 1.895161E+01 1.646235E+01 1.526771E+01 1.461224E+01 1.426106E+01
1.411578E+01 1.413655E+01 1.432954E+01 1.474505E+01 1.552409E+01 1.708716E+01
2.120639E+01 4.134021E+01
IZ = 12
3.056245E+01 1.897832E+01 1.648483E+01 1.528787E+01 1.462979E+01 1.427567E+01
1.412740E+01 1.414545E+01 1.433595E+01 1.474913E+01 1.552587E+01 1.708700E+01
2.120803E+01 4.135176E+01
IZ = 13
3.057605E+01 1.898747E+01 1.649220E+01 1.529348E+01 1.463359E+01 1.427761E+01
1.412745E+01 1.414354E+01 1.433231E+01 1.474378E+01 1.551892E+01 1.707856E+01
2.119772E+01 4.133514E+01
IZ = 14
3.056647E+01 1.898558E+01 1.648982E+01 1.528864E+01 1.462644E+01 1.426832E+01
1.411598E+01 1.412970E+01 1.431587E+01 1.472492E+01 1.549795E+01 1.705536E+01
2.116743E+01 4.127612E+01
IZ = 15
3.054459E+01 1.897516E+01 1.647749E+01 1.527084E+01 1.460374E+01 1.424127E+01
1.408453E+01 1.409330E+01 1.427412E+01 1.467825E+01 1.544703E+01 1.700038E+01
2.109823E+01 4.114791E+01
IZ = 16
3.051914E+01 1.895714E+01 1.645088E+01 1.522852E+01 1.454869E+01 1.417548E+01
1.400816E+01 1.400446E+01 1.417142E+01 1.456279E+01 1.532093E+01 1.686545E+01
2.093313E+01 4.088929E+01
IZ = 17
3.037306E+01 1.891447E+01 1.638658E+01 1.512567E+01 1.441558E+01 1.401884E+01
1.382721E+01 1.379110E+01 1.391787E+01 1.426794E+01 1.498711E+01 1.649489E+01
2.049078E+01 4.039200E+01
IZ = 18
3.257338E+01 1.929100E+01 1.635999E+01 1.490406E+01 1.410995E+01 1.368523E+01
1.346347E+01 1.334920E+01 1.334774E+01 1.354982E+01 1.410954E+01 1.542228E+01
1.909419E+01 3.893631E+01
*****
END OF INTERFACE DATA

```

6. CONCLUSIONS

The results showed good quantitative agreement with analytical data though several sweeps are need to guarantee the convergence. Although the resulting shear stress profile for de $k-\omega$ turbulence model seems to fit better near the walls, it was more unstable and harder to converge than the standard $k-\epsilon$ one.

Also, it was verified that near the open borders of the plate the shear stress is usually higher because of an increase in the turbulence effects at these elements. This causes the average shear stress to have sometimes twice the value than in the remaining elements. It was important to point out that the shear stress near the borders seems to be over-predicted and unfortunately it was impossible to check experimentally this data.

Most of the turbulence models currently implemented in PHOENICS seems to be able to predict reasonable values only near the wall or in the bulk. It would be very interesting to study and implement a new turbulence approach that can deal with the same accuracy in all regions.

Finally this case was used as a base for a general q1 template and implemented in a Human-Machine Interface (HMI) in order to turn typical sensibility analysis into an easy task, allowing series of tests to be performed with very few clicks of the mouse. This enables even new users or equipment designers who may wish not to invest in training in PHOENICS to perform similar studies [Ref. 3].

7. BIBLIOGRAPHY

1. Bird, R. Byron et al. (1976) "*Transport Phenomena*", John Wiley & Sons, Wiley International Edition.
2. Perry, R., Green, D.W. (1997) "*Perry's Chemical Engineer's Handbook*", McGraw Hill, 7th Ed.
3. Serfaty, R. et al. (2000) "*Development of an Application Oriented Interface for PHOENICS*", The PHOENICS Journal of Computational Fluid Dynamics and its Applications, Vol. 13, No. 2, pp 204-210.